

# Breast Ultrasound Computer-Aided Diagnosis Using Structure-Aware Triplet Path Networks

Erlei Zhang<sup>1,2</sup>, Zi Yang<sup>2</sup>, Stephen Seiler<sup>3</sup>, Mingli Chen<sup>2</sup>, Weiguo Lu<sup>2</sup>, Xuejun Gu<sup>2</sup>(✉)

<sup>1</sup> Northwest University, Xi'an, Shaanxi, China

<sup>2</sup> Medical Artificial Intelligence and Automation Laboratory, Department of Radiation Oncology, University of Texas Southwestern Medical Center, Dallas, USA

<sup>3</sup> Department of Radiology, University of Texas Southwestern Medical Center, Dallas, USA  
Xuejun.Gu@UTSouthwestern.edu

**Abstract.** Breast ultrasound (US) is an effective imaging modality for breast cancer detection and diagnosis. The structural characteristics of breast lesion play an important role in Computer-Aided Diagnosis (CAD). In this paper, a novel structure-aware triplet path networks (SATPN) was designed to integrate classification and two image reconstruction tasks to achieve accurate diagnosis on US images with small training dataset. Specifically, we enhance clinically-approved breast lesion structure characteristics through converting original breast US images to BIRADS-oriented feature maps (BFMs) with a distance-transformation coupled Gaussian filter. Then, the converted BFMs were used as the inputs of SATPN, which performed lesion classification task and two unsupervised stacked convolutional Auto-Encoder (SCAE) networks for benign and malignant image reconstruction tasks, independently. We trained the SATPN with an alternative learning strategy by balancing image reconstruction error and classification label prediction error. At the test stage, the lesion label was determined by the weighted voting with reconstruction error and label prediction error. We compared the performance of the SATPN with TPN using original image as input and our previous developed semi-supervised deep learning methods using BFMs as inputs. Experimental results on two breast US datasets showed that SATPN ranked the best among the three networks, with classification accuracy around 93.5%. These findings indicated that SATPN is promising for effective breast US lesion CAD using small datasets.

**Keywords:** Breast Cancer, Ultrasound, Computer-Aided Diagnosis, BIRADS Features, Semi-supervised Deep Learning.

## 1 Introduction

Breast cancer is the most common malignancy in women in the United States and the second leading cause of cancer death for women worldwide. Breast ultrasound (US) is a widely adopted early breast cancer diagnosis imaging modality that has the advantages of being non-invasive, safe, and relatively inexpensive [1]. Many studies have applied computer-aided diagnosis (CAD) to breast US to assist radiologists and

improve diagnostic accuracy [2]. Traditional US CAD systems, most of the features are hand-crafted [3, 4], which have limited accuracy due to the variation of lesion characteristics and image acquisition. Recently, deep learning (DL) provides a way to automatically learn discriminative features from raw data [5] and has been widely adopted in medical image analysis, including breast US CAD diagnosis [6].

However, direct training of deep networks on relatively small image datasets is prone to overfitting. To mitigate this issue, researchers integrated unsupervised deep stacked auto-encoder (AE)-based methods for high-level features extraction and supervised fine-tuning for breast US image classification [7]. Such combination has its deficits: 1) AE extracted features may not be suitable for classification: If AE merely extracts features on the natural characters of the data without considering the label information in the pre-training phase, the extracted features have no ability for describing the given categories, which poses difficulties when applied to classification. 2) The image intensity based  $\ell_2$  norm cost function cannot catch lesion structure attributes:  $\ell_2$  norm correlates poorly with image quality as perceived by a human observer [8] since it doesn't consider the shape, contour attributes of breast lesion which play important roles in breast diagnosis. 3) Sharing the same AE architecture for image restoration is difficult to catch the variation between benign and malignant lesion: Lesions' structural variations within benign class are smaller than those within malignant class. Building two separate expert systems for benign and malignant lesion image restoration is necessary.

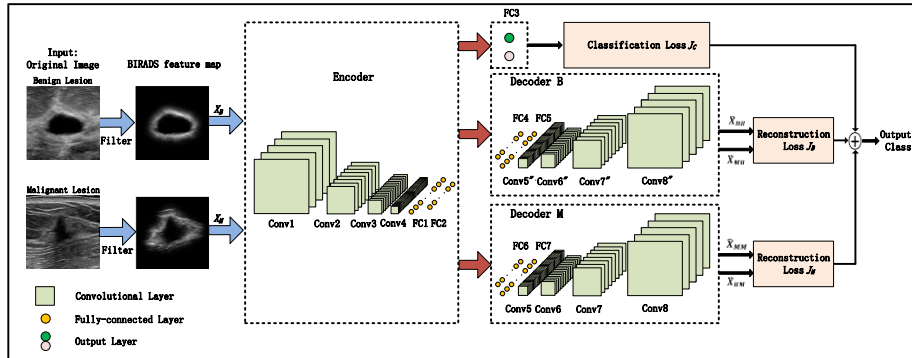


**Fig. 1.** Illustration of SATPN architecture. The extracted BFM s are used as the input of SATPN, which is characterized as two unsupervised SCAE networks for benign and malignant image reconstruction, independently, along with lesion classification.

In this paper, we report a novel structure-aware triplet path networks (SATPN) (architecture shown in Fig. 1) that incorporates the clinical knowledge of lesion characteristics (BIRADS features) and triplet path networks with the structural similarity index (SSIM) to achieve accurate diagnosis on breast US images. The breast US images are converted to BIRADS-oriented feature maps (BFMs) using a distance-transformation coupled Gaussian filter (DTGF). The BFM s not only keep the original US image information, but they also enhance structure characteristics (shape, lesion boundary, undulation, and angular characteristics) of the lesion. Then, the BFM s are used as the inputs of the SATPN, which performs a multi-task learning by integrating

two stacked convolutional auto-encoder (SCAE)-based unsupervised image feature extraction and diagnosis-oriented supervised lesion classification. This integrated multi-path network allows SCAE (SSIM as cost function) to independently extract image features of benign and malignant lesions with the constraints from the lesion classification task, while the lesion classification is achieved by utilizing the SCAE encoder features with a convolutional network. In the end, lesions are classified by the weighted voting of reconstruction errors and label prediction errors.

## 2 Method

### 2.1 BIRADS Oriented Feature Maps

Breast Imaging Reporting and Data System (BIRADS), was proposed to help radiologists to describe and evaluate breast lesions [4]. Computerized BIRADS features, shape, lesion boundary, abrupt degree, undulation and angular characteristics of lesion have a high correlation with the pathological results. The undulation and the angular characteristics are reflected in the lesion boundary as shown in Fig. 2(b).

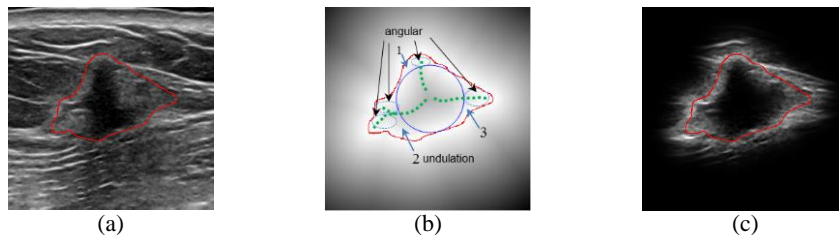


**Fig. 2.** An example of BIRADS oriented feature map: (a) A malignant lesion with boundary (red line); (b) Undulation and angular characteristics; (c) An example of BFM.

We convert lesion boundary into BFM which are defined as follows:

$$BFMs = I(P) \cdot e^{-\frac{Dist(P)^2}{\sigma^2}} \quad (1)$$

where  $Dist(P) = \min\{ED(p, q_i)\}$  is the transformed distance, with  $i = 1, \dots, n$ . Here  $p$  is a pixel in an image, and  $q_i$  is a pixel on the boundary forming by  $n$  points and  $ED(p, q_i)$  is Euclidean distance between pixel  $p$  and  $q_i$ .  $\sigma$  is a parameter used to control the width of the part of surrounding tissue near the boundary. Fig. 2(c) shows an example of BFM with lesion boundary and key areas near the boundary highlighted.

### 2.2 Structure-aware Triplet Path Networks

A novel SATPN is developed as shown in Fig. 1. The converted BFM are used as the input of the SATPN, which integrates image feature extraction through two unsupervised image reconstruction pipelines and a supervised lesion classification pipeline.

The image reconstruction pipelines are similar to the standard SCAE structure, which consists of an encoder and a decoder, as shown in Fig. 1. We build two image reconstruction pipelines, one for benign lesion image and the other malignant lesion

image. The benign pipeline is designed to well restore the benign images but poor recover the malignant images with an objective function:

$$\min_{\theta_B} J_B = \frac{1}{N_i} \sum_{i=1}^{N_i} \text{loss}_r(\mathbf{x}_B^{(i)}, \hat{\mathbf{x}}_{BB}^{(i)}) - \frac{\alpha}{N_j} \sum_{j=1}^{N_j} \text{loss}_r(\mathbf{x}_M^{(j)}, \hat{\mathbf{x}}_{MB}^{(j)}) + \gamma \cdot \mathbf{R}(\theta_B) \quad (2)$$

While the malignant pipeline does the opposite, well in the malignant images restore but poor in the benign images recover. The objective function is as follows:

$$\min_{\theta_M} J_M = \frac{1}{N_j} \sum_{j=1}^{N_j} \text{loss}_r(\mathbf{x}_M^{(j)}, \hat{\mathbf{x}}_{MM}^{(j)}) - \frac{\alpha}{N_i} \sum_{i=1}^{N_i} \text{loss}_r(\mathbf{x}_B^{(i)}, \hat{\mathbf{x}}_{BM}^{(i)}) + \gamma \cdot \mathbf{R}(\theta_M) \quad (3)$$

where  $\mathbf{x}_B^{(i)}$  and  $\mathbf{x}_M^{(j)}$  denotes benign and malignant samples,  $\hat{\mathbf{x}}_{BB}^{(i)}$  and  $\hat{\mathbf{x}}_{MB}^{(j)}$  are reconstructions of  $\mathbf{x}_B^{(i)}$  and  $\mathbf{x}_M^{(j)}$  in benign pipeline,  $\hat{\mathbf{x}}_{MM}^{(j)}$  and  $\hat{\mathbf{x}}_{BM}^{(i)}$  are reconstructions of  $\mathbf{x}_B^{(i)}$  and  $\mathbf{x}_M^{(j)}$  in malignant pipeline. The reconstruction loss function uses the SSIM [9]:  $\text{loss}_r(\mathbf{x}, \hat{\mathbf{x}}) = 1 - \text{SSIM}(\mathbf{x}, \hat{\mathbf{x}})$ . The loss functions are regularized by  $\mathbf{R}(\theta_B) = \|\mathbf{W}_{en}\|_2^2 + \|\mathbf{W}_{Bde}\|_2^2$ ,  $\mathbf{R}(\theta_M) = \|\mathbf{W}_{en}\|_2^2 + \|\mathbf{W}_{Mde}\|_2^2$ .  $\{\alpha, \gamma\} \in [0, 1]$  are two parameters to balance each terms.

The lesion classification task is implemented by an encoder network and a classifier as shown in Fig. 1, which can be expressed as

$$\begin{cases} \mathbf{h} = \mathbf{W}_{en} * \mathbf{x} + \mathbf{b}_{en} \\ \hat{\mathbf{y}} = \mathbf{f}_c(\mathbf{h}, \boldsymbol{\beta}) \end{cases} \quad (4)$$

where  $\mathbf{h}$  is the output of the encoder,  $\mathbf{f}_c(\cdot)$  is a softmax classifier, and  $\boldsymbol{\beta}$  is a vector of parameters of the classifier to be learned.  $\hat{\mathbf{y}} \in \mathfrak{R}^K$  is the output of the classifier and ranges within  $[0, 1]$ . The objective function of classification is

$$\min_{\theta_C} J_C = \frac{1}{N} \sum_{n=1}^N \text{loss}_c(\mathbf{y}^{(n)}, \hat{\mathbf{y}}^{(n)}) + \gamma \cdot \mathbf{R}(\theta_C) \quad (5)$$

where  $\mathbf{y}^{(n)}$  denotes sample labels,  $\theta_C = [\mathbf{W}_{en}, \mathbf{b}_{en}; \boldsymbol{\beta}]$  is learning or tuning by the training dataset. Commonly, the loss function  $\text{loss}_c(\cdot)$  uses cross-entropy.

Combining classification and image reconstruction pipelines, the objective function of SATPN is as follows:

$$\min_{\theta} \lambda \cdot (J_B + J_M) + (1 - \lambda) \cdot J_C \quad (6)$$

where  $\theta = [\theta_B, \theta_M, \theta_C]$  and  $\lambda \in [0, 1]$  are used to balance the classification and reconstruction tasks. During feature learning, the encoding parameters are shared among three tasks, while the decoding parameters only participate in the reconstruction tasks. The objective function can be achieved by alternately learning [10].

At the test stage, the lesion  $\mathbf{x}$  was classified by the combination of reconstruction error and label prediction error:

$$\hat{\mathbf{y}} = \min_{0,1} \{-\ln(P_{CB} \cdot P_{rB}), -\ln(P_{CM} \cdot P_{rM})\} \quad (7)$$

where  $P_{CB}$  and  $P_{CM}$  are the class probability estimates from classification pipeline,  $\hat{\mathbf{x}}_B$  and  $\hat{\mathbf{x}}_M$  are two outputs of two construction pipelines,  $P_{rB} = \text{SSIM}(\mathbf{x}, \hat{\mathbf{x}}_B) / (\text{SSIM}(\mathbf{x}, \hat{\mathbf{x}}_B) + \text{SSIM}(\mathbf{x}, \hat{\mathbf{x}}_M))$ ,  $P_{rM} = \text{SSIM}(\mathbf{x}, \hat{\mathbf{x}}_M) / (\text{SSIM}(\mathbf{x}, \hat{\mathbf{x}}_B) + \text{SSIM}(\mathbf{x}, \hat{\mathbf{x}}_M))$ .

In this paper, the classification pipeline has four convolutional layers: 8(Conv1), 16(Conv2), 32(Conv3), and 64(Conv4) @3×3 filters, four max-pooling layers of size 2×2 after each convolutional layer, and three fully-connected layers (FC1, FC2, FC3),

as shown in Fig. 1. The number of neurons in FC1 and FC2 is 256 and 64, respectively. The output layer FC3 has a softmax activation function with two neurons. The dropout (with a probability of 0.5) is applied after FC1 and FC2 to prevent overfitting. ReLU activations are used in all hidden layers. The two reconstruction pipelines have an encoder and a decoder, respectively. The encoder is shared with the classification pipeline, including the four convolutional layers (Conv1, Conv2, Conv3, and Conv4) and two fully-connected layers (FC1 and FC2). The decoder has the inverse configuration of the encoder, including two fully-connected layers (FC4 and FC5, FC6 and FC7), four pairs of convolution and upsampling layers, and a convolutional output layer with linear activations. The classification and two reconstruction tasks are alternately updated via Adam with a learning rate of  $3 \times 10^{-4}$  and stopping to update the network when the average reconstruction loss remains stable. The parameters ( $\alpha=0.1$ ,  $\gamma=0.01$ , and  $\lambda=0.5$ ) are set according to accuracy on the validation data.

### 3 Experimental Results

#### 3.1 Experimental Setup

**Dataset I:** A public breast B-Mode US image dataset, UDIAT [11]. In this study, 160 images were selected and cropped to  $256 \times 256$  centered on the lesions. These 160 images include 53 images with malignant lesions and 107 with benign lesions. 50% samples are randomly selected from benign and malignant lesions as the training set and the rest 50% samples are used as the testing set.

**Dataset II:** The in-house clinical dataset, UTSW dataset, is a B-mode US breast image dataset collected with a Philips iU22 scanner. The lesions were identified as benign or malignant based on the pathologic examination of a subsequent biopsy. In this study, we selected 295 images including 205 benign lesions and 90 malignant lesions. The images were resampled to a resolution of 0.084mm and cropped to  $256 \times 256$  centered on the lesions. We used a marker-controlled watershed segmentation method [12] to create the tumor boundary. 80% per class of samples are randomly chosen to construct a training set, and 20% of samples are randomly chosen as the test set.

To demonstrate the effectiveness of SATPN, we compare its performance with 1) ORI-TPN which uses original images, not BFMs, as input, and 2) our previous developed BIRADS-SDL [13], a semi-supervised deep learning which performs SCAE image reconstruction guided by lesion classification. In this paper, ACC, AUC, and MCC represent three performance metrics: accuracy, area under receiver operating characteristic curve, and Matthews correlation coefficient, respectively [14].

#### 3.2 Classification Results on Single Dataset

Table 1 shows the classification results (mean  $\pm$  standard deviation of ten runs) for three methods on the UDIAT and UTSW datasets. First, comparing the methods with different inputs (ORI- and BIRADS-based methods), we found that BIRADS-based methods outperformed ORI-based methods from the perspective of the three metrics. The BIRADS-based methods achieved ACC, AUC, and MCC values about 5%, 7%,

and 10% higher, respectively, than the ORI-based methods, which indicates the advantage of using BIRADS-oriented feature maps. Second, we found SATPN obtained better results than BIRADS-SDL method, which means they learn more effective classification features by building two separate expert systems for benign and malignant lesion image reconstruction. Final, the proposed SATPN produces the best diagnosis results than other compared methods by taking advantage of the structural characteristics of lesions. Similar conclusions can be drawn from the classification results on the UTSW dataset. SATPN outperformed the other compared methods in terms of ACC, AUC, and MCC. Unlike the UDIAT dataset, SATPN only outperformed the other methods in terms of ACC by about 2%. One reason for this might be that the lesion boundary produced by auto-segmentation is not accurate, which would reduce the classification accuracy.

**Table 1.** Classification results (mean  $\pm$  std%) of different methods on UDIAT & UTSW dataset

Method	UDIAT			UTSW		
	ORI-TPN	BIRADS-SDL	SATPN	ORI-TPN	BIRADS-SDL	SATPN
ACC	87.88 $\pm$ 2.31	92.00 $\pm$ 2.38	<b>93.75<math>\pm</math>1.75</b>	83.05 $\pm$ 1.28	83.90 $\pm$ 3.81	<b>85.25<math>\pm</math>3.13</b>
AUC	82.81 $\pm$ 5.06	88.98 $\pm$ 2.51	<b>90.12<math>\pm</math>1.20</b>	74.22 $\pm$ 5.83	<b>79.62<math>\pm</math>3.48</b>	79.57 $\pm$ 3.06
MCC	70.36 $\pm$ 6.79	82.07 $\pm$ 5.02	<b>84.41<math>\pm</math>2.19</b>	56.28 $\pm$ 9.21	60.73 $\pm$ 6.88	<b>64.63<math>\pm</math>5.29</b>

### 3.3 Model Validation across Dataset

We evaluated the generality of SATPN through experiments with cross-dataset, including 1) training models on one dataset and testing on the other dataset; 2) training models on both datasets and testing on each dataset respectively.

Firstly, each method is trained on UDIAT dataset (randomly select 50% samples) and testing on UTSW dataset (randomly select 20% samples). The proposed SATPN produces acceptable results (ACC, AUC and MCC  $\sim$ 84.92 $\pm$ 2.98%, 76.51 $\pm$ 5.08%, and 60.05 $\pm$ 7.49%) which are better than other methods' results where the ACC values less than 80%. It means that SATPN is generalizable across the different US devices and institutions without overfitting to a single dataset and achieved satisfactory results. Further, we also trained each method on UTSW (randomly select 80% samples) and tested on UDIAT dataset (randomly select 50% samples). The classification accuracy of all the methods appears significantly decrease compared with Table 1. One reason is that there are some differences between two datasets collected by different manufactures device; another reason might be the model trained with UTSW dataset has a limited generality due to the limited samples and imprecise boundaries of the lesions.

Further, each method was trained on the combined UDIAT (randomly selected 50% of the samples) and UTSW datasets (randomly selected 80% of the samples), then tested on the remaining samples from each dataset, respectively. All the methods produced results similar to those shown in Table 1, and the proposed SATPN performed the best in all the comparisons. This indicates that SATPN method is more generalizable across different datasets without overfitting to single institution data.

### 3.4 Effects of Gaussian Filter Parameter $\sigma$

For UDIAT dataset, the overall accuracy variations of classification results of two BIRADS-based methods across  $\sigma$  values are shown in Fig. 3. It can be seen that SATPN almost has higher accuracy than BIRADS-SDL across all the  $\sigma$  values although it has some fluctuations. All the curves show the best results at  $\sigma = 20$ , and a slightly decreased with smaller value or larger value. Also, the standard deviation varies are relatively small around  $\sigma = 20$ . This indicates that the area in the certain range of lesion boundary play a most important role for lesion classification.

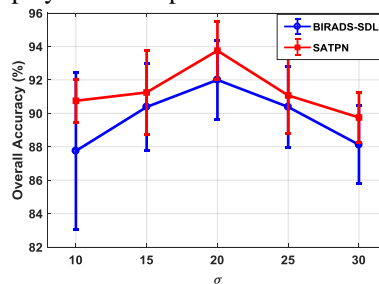


Fig. 3. Effect of parameter  $\sigma$  in Gaussian filter on BIRADS-based methods.

## 4 Discussion and Conclusion

We developed a new SATPN method to incorporate structural characteristics of breast lesion into triplet path deep neural networks for accurate diagnosis on US images with relatively small training dataset. The effectiveness of SATPN has been verified on two breast US image datasets and achieved high diagnostic accuracy.

Unlike traditional machine learning methods [15], SATPN automatically learned representative and discriminative features by hierarchical deep neural network. Different from the recent DL methods with pre-training technique or transfer learning [16], we focus on the structural characteristics of the breast lesion through fusing the existing conventional BIRADS features into triplet path deep neural network with SSIM as the cost function, improves performance in breast lesion diagnosis. In our case, the SATPN only used 80 labeled images for training the network, and all the results (ACC and AUC ~93% and 90%) are comparable with the results reported in recent papers [16, 17], where the AUC values are around 85% and the networks are trained with bigger dataset for training.

Then, the generality of SATPN was evaluated through experiments with cross-dataset. In our experiments, two datasets came from different medical centers and manufacturers. When training model on the collection of two datasets, the proposed SATPN generalizes across the difference produced by manufacturer and institution without overfitting to a single dataset and achieves satisfactory results. Although the model is learned from one dataset and testing on the other different dataset, it still ranked the best performance among the six comparing networks.

In summary, the proposed SATPN achieves the best results among all the compared methods in each case and has the capacity to deal with multiple different da-

tasets under one model, which indicated that SATPN is promising for effective breast US lesion CAD using small datasets.

## References

1. Cheng, H.-D., Shan, J., Ju, W., Guo, Y., Zhang, L.: Automated breast cancer detection and classification using ultrasound images: A survey. *Pattern recognition* 43, 299-317 (2010)
2. Huang, Q., Zhang, F., Li, X.: Machine learning in ultrasound computer-aided diagnostic systems: a survey. *BioMed research international* 2018, (2018)
3. Shen, W.-C., Chang, R.-F., Moon, W.K., Chou, Y.-H., *et al.*: Breast ultrasound computer-aided diagnosis using BI-RADS features. *Academic radiology* 14, 928-939 (2007)
4. Flores, W.G., de Albuquerque Pereira, W.C., *et al.*: Improving classification performance of breast lesions on ultrasonography. *Pattern Recognition* 48, 1125-1136 (2015)
5. LeCun, Y., Bengio, Y., Hinton, G.: Deep learning. *nature* 521, 436 (2015)
6. Shen, D., Wu, G., Suk, H.-I.: Deep learning in medical image analysis. *Annual review of biomedical engineering* 19, 221-248 (2017)
7. Cheng, J.-Z., Ni, D., Chou, Y.-H., Qin, J., Tiu, C.-M., Chang, Y.-C., Huang, C.-S., *et al.*: Computer-aided diagnosis with deep learning architecture: applications to breast lesions in US images and pulmonary nodules in CT scans. *Scientific reports* 6, 24454 (2016)
8. Zhao, H., Gallo, O., Frosio, I., Kautz, J.: Loss functions for image restoration with neural networks. *IEEE Transactions on Computational Imaging* 3, 47-57 (2017)
9. Wang, Z., Bovik, A.C., Sheikh, H.R., Simoncelli, E.P.: Image quality assessment: from error visibility to structural similarity. *IEEE transactions on image processing* 13, 600-612 (2004)
10. Ghifary, M., Kleijn, W.B., Zhang, M., Balduzzi, D., Li, W.: Deep reconstruction-classification networks for unsupervised domain adaptation. In: *European Conference on Computer Vision*, pp. 597-613. Springer, (2016)
11. Yap, M.H., Pons, G., Martí, J., Ganau, S., Sentís, M., Zwiggelaar, R., Davison, A.K., Martí, R.: Automated breast ultrasound lesions detection using convolutional neural networks. *IEEE journal of biomedical and health informatics* 22, 1218-1226 (2018)
12. Gomez, W., Leija, L., Alvarenga, A., Infantosi, A., Pereira, W.: Computerized lesion segmentation of breast ultrasound based on marker-controlled watershed transformation. *Medical physics* 37, 82-95 (2010)
13. Zhang, E., Seiler, S., Chen, M., Lu, W., Gu, X.: BIRADS Features-Oriented Semi-supervised Deep Learning for Breast Ultrasound Computer-Aided Diagnosis. *arXiv preprint arXiv: 2635960*, (2019)
14. Zhou, H., Gao, M., Skolnick, J.: ENTPRISE: an algorithm for predicting human disease-associated amino acid substitutions from sequence entropy and predicted protein structures. *PLOS one* 11, e0150965 (2016)
15. Jalalian, A., Mashohor, S.B., Mahmud, H.R., Saripan, M.I.B., Ramli, A.R.B., Karasfi, B.: Computer-aided detection/diagnosis of breast cancer in mammography and ultrasound: a review. *Clinical imaging* 37, 420-426 (2013)
16. Antropova, N., Huynh, B.Q., Giger, M.L.: A deep feature fusion methodology for breast cancer diagnosis demonstrated on three imaging modality datasets. *Medical physics* 44, 5162-5171 (2017)
17. Byra, M.: Discriminant analysis of neural style representations for breast lesion classification in ultrasound. *Biocybernetics and Biomedical Engineering* (2018)